Coherent Control of Retinal Isomerization in Bacteriorhodopsin

Valentyn I. Prokhorenko, *et al.*

Science **313**, 1257 (2006);
DOI: 10.1126/science.1130747

Coherent Control of Retinal Isomerization in Bacteriorhodopsin

Valentyn I. Prokhorenko,[1] Andrea M. Nagy,[1] Stephen A. Waschuk,[2] Leonid S. Brown,[2] Robert R. Birge,[3] R. J. Dwayne Miller[1]*

Optical control of the primary step of photoisomerization of the retinal molecule in bacteriorhodopsin from the all-trans to the 13-cis state was demonstrated under weak field conditions (where only 1 of 300 retinal molecules absorbs a photon during the excitation cycle) that are relevant to understanding biological processes. By modulating the phases and amplitudes of the spectral components in the photoexcitation pulse, we showed that the absolute quantity of 13-cis retinal formed upon excitation can be enhanced or suppressed by ±20% of the yield observed using a short transform-limited pulse having the same actinic energy. The shaped pulses were shown to be phase-sensitive at intensities too low to access different higher electronic states, and so these pulses apparently steer the isomerization through constructive and destructive interference effects, a mechanism supported by observed signatures of vibrational coherence. These results show that the wave properties of matter can be observed and even manipulated in a system as large and complex as a protein.

Quantum mechanics dictates that all matter has an inherent wave property. On a molecular scale, this property can lead to destructive and constructive interferences that have a pronounced effect on transmission probabilities along reaction coordinates. Modern spectroscopic techniques have afforded direct evidence of such interferences and even exploited interference of the underlying wave properties to steer chemical reactions one way or another (*1*). For the most part, however, these studies have focused on small molecules and ions. In a protein, random fluctuations among the enormous number of degrees of freedom might be expected to cancel any interference effects. At the same time, proteins are highly evolved structures, and the question arises whether the phases of the underlying matter waves could play a role or even be manipulated in directing biological processes. This question can be addressed by determining the degree of conserved phase relationships, or quantum coherence, involved in a chemical process occurring within the confines of the protein environment. Experimental tests for coherence, as for any wave phenomena, must be able to demonstrate the creation of both constructive and destructive interference pathways, a process termed coherent control for molecular systems (*1*, *2*).

Tests of quantum coherence are most readily accomplished for photoactive processes in which short, specifically shaped excitation pulses can be used to manipulate the process on a time scale faster than random thermal motions act to scramble phase relationships (cause decoherence). In this regard, one of the fastest biological processes is the photoisomerization of the retinal molecule in rhodopsin proteins. This relatively simple photochemical reaction is the primary event for vision in higher organisms, photoreceptor response, and energy conversion in halobacteria. As such, the reaction has been subject to intense experimental and theoretical investigation (*3*–*11*). The possibility of manipulating the isomerization efficiency by excitation with tailored excitation light pulses has also been discussed from a theoretical standpoint in which a small subset of the total number of coupled motions is treated (*12*, *13*). However, the full problem is computationally intractable and so requires direct experimental investigation for resolution.

Experimental manipulation of the relative photoisomerization yield of a molecule was recently reported for the cyanine dye NK88 in solution (*14*). These studies were conducted using excitation energies near saturation level for the absorption in question (1.5 μJ per pulse); the primary action of the shaped light fields may have been to control the excited-state population (*15*) rather than the reaction coordinate itself. Under strong field excitation conditions, multiphoton processes inevitably access higher-lying excited states and so substantially perturb the state of interest. These issues are irrelevant if the objective is to induce a particular reaction outcome, but they become important in interpreting the correlation of the pulse shapes with the molecular processes.

Previous pulse-shaping studies of biological systems (*16*) were also performed under relatively strong excitation conditions and demonstrated the quenching of energy transfer from the carotenoids in light-harvesting systems. This effect was attributed to enhanced nonradiative relaxation of the carotenoid excited state; it was not possible to control the converse pathway to increase energy transfer. Our goal in the present study was to control the absolute isomerization yield of the 13-cis retinal isomer in bacteriorhodopsin (bR). We sought specifically to control the degree of coherence in the protein environment in the weak field regime so as to ensure that the resultant dynamics would pertain to the protein's behavior under normal functional conditions. In this context, we report the manipulation of the absolute yield of 13-cis retinal over a 40% range, clearly demonstrating that a protein can manifest coherent interference effects. Through feedback-controlled amplitude and phase variation of the spectral components composing the excitation pulse, we could selectively enhance or suppress the isomerization yield by 20% in either direction.

Optimization of the isomerization yield. Photoisomerization of the retinal chromophore in bR (Fig. 1) occurs with a relatively high quantum yield (≈65%) (*17*, *18*) of the 13-cis isomer. Prior work has shown that the isomerization is complete within ≈3 ps (*6*), and the product, termed the K intermediate, has a well-resolved positive differential absorption (ΔA) band in the 630- to 640-nm range (*19*, *20*). To ensure adequate vibrational cooling, we chose a 20-ps delay after the actinic pulse before targeting the 630-nm absorption feature for optimization (a detailed description of the materials and methods is given in the supporting online material). At this delay, the magnitude of measured signal ΔA, weighted by actinic excitation energy (the amount of photons absorbed in a sample), directly reflects the isomerization

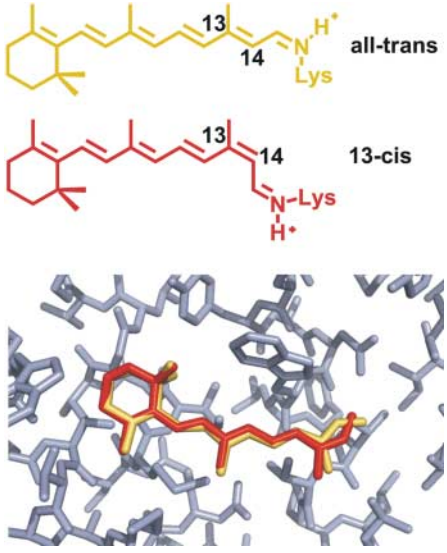

Fig. 1. Configurations of the retinal molecule (**top**) in bacteriorhodopsin (**bottom**) in the ground state (all-trans, yellow), and after isomerization (13-cis K form, red). [The bottom image is from the Protein Data Bank; identification numbers 1QHJ and 1QKP (*39*).] The photoisomerization process requires a torsional motion and bond stretching along the C13-C14 axis. The motion through the transition-state region connecting the excited reactant and product surfaces will involve a superposition of vibrations to give this localized displacement (*11*, *12*).

[1]Institute for Optical Sciences, Departments of Chemistry and Physics, University of Toronto, 80 St. George Street, M5S3H6, Toronto, Ontario, Canada. [2]Department of Physics, University of Guelph, N1G2W1, Guelph, Ontario, Canada. [3]Department of Chemistry, University of Connecticut, Storrs, CT, USA.

*To whom correspondence should be addressed. E-mail: dmiller@lphys.chem.utoronto.ca.

yield. We then used a well-established genetic algorithm and feedback approach to solve a multivariable problem to converge toward tailored pulses that would either maximize or minimize the 630-nm induced absorption, corresponding to the respective enhancement or suppression of the isomerization yield (Fig. 2). The different excitation pulse shapes were generated by appropriate manipulation of incoming transform-limited pulses [19 fs full width at half maximum (FWHM), centered at 565 nm with a bandwidth of 60 nm] in both frequency and phase domains (*21*). Using only phase manipulation would substantially restrict the control space. In accordance with certain properties of the Fourier transform, frequency amplitude modulation is necessary to produce, for example, a comb of temporally spaced subpulses, a prominent feature of the optimal pulses derived in recent coherent control experiments (*16*, *22*).

We applied the optimization algorithm to a starting set of 30 pulses with randomly distributed spectral phases and amplitudes (pulse energies were 16 to 17 nJ, corresponding to a fluence E_{exc} = 2.7 × 10^{14} photons/cm^2); the growth of ΔA consistently saturates after 30 to 40 generations (600 to 800 shaping cycles) at a level ~23% higher than that induced by the excitation with the transform-limited pulse. The spectrum of the optimal excitation pulse (Fig. 3A) has a gravity center at ~557 nm and a regular structure composed of several peaks spaced ~6 nm apart (both of these features have been reproduced in more than 20 optimization experiments). The anti-optimization experiment (Fig. 2B) also converged after ~30 generations under the same conditions, to yield a pulse that suppresses isomerization efficiency by ~24%. The spectrum of the anti-optimal pulse (Fig. 3D) was relatively broad and redshifted to ~577 nm. The isomerization quantum yield of 13-cis retinal in bR has been shown experimentally to be wavelength-independent across the full 500- to 670-nm absorption band. This spectral insensitivity was confirmed at different temperatures, using different light sources and methods (*23*–*26*). Nevertheless, we performed an additional check by irradiating our bR samples with tunable 120- to 140-fs excitation pulses of relatively narrow spectral width (8 nm FWHM), and found the yield to be wavelength-independent within a 535- to 610-nm window (fig. S2). The optimization has to be ascribed to the specific shapes of the excitation pulses.

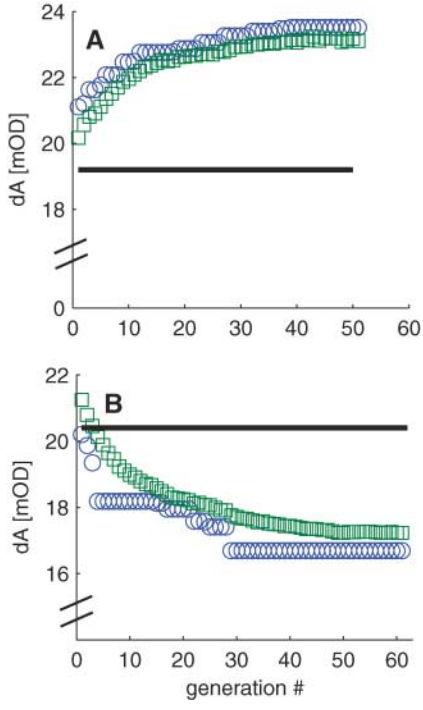

Fig. 2. Effect of evolving pulse shapes on the isomerization yield of retinal in bR, measured at 630 nm delayed 20 ps after excitation. In (**A**) maximization and (**B**) minimization experiments, green squares correspond to averaged values of the differential absorbance ΔA (over the whole population), and blue circles correspond to the most effective pulses [for enhancement in (A) or suppression in (B)] within the current population. The solid horizontal lines correspond to the ΔA measured by excitation with the transform-limited pulse (19 fs FWHM) as a baseline for comparison.

For determining the temporal profiles of the optimized pulses, we used frequency-resolved optically gated (FROG) measurements (Fig. 3). Both optimal and anti-optimal pulses displayed regular and periodic modulations. The retrieved intensity profile of the optimal pulse showed a comb of ~eight subpulses (Fig. 3C). In contrast, energy in the anti-optimal pulse was mostly concentrated in a single feature ~80 fs (FWHM) in duration (Fig. 3F), with smaller-amplitude subpulses. These intensity profiles were independently examined by recording the cross-correlation functions between the investigated pulses and a compressed white-light pulse (harmonic sum generation, with detection corresponding to the doubled frequency of the pulses) and were in good agreement with the retrieved pulse profiles from the FROG measurements.

Regarding frequency distributions over time, distinct spectral components in the optimal pulse had different magnitudes (and signs) of chirp (Fig. 3C), whereas the main peak in the anti-optimal pulse was not chirped (Fig. 3F). In our previous studies of the population transfer in solvated molecules, an anti-optimal pulse that suppressed the excited-state population had a clear, strong, negative chirp (*22*). Lack of this feature in the present case implies that suppression of the isomerization yield in bR is caused not by lowering of the excited-state population but by some process that affects the reaction probability; namely, destructive interference effects in the excited vibrational modes. This interpretation was independently confirmed by measuring the number of absorbed photons directly (the absorbed energy was measured as the difference between incoming and outgoing pulse energies, using a power meter with a corresponding correction for wavelength). To an accuracy of ±1%, the number of absorbed photons was found to be the same for the optimal, transform-limited, and anti-optimal pulses at low excitations, where the response of the bR is linear with respect to absorbed energy. Because the number of absorbed photons exactly corresponds to the number of excited molecules in this low excitation limit, we therefore conclude that the observed changes in isomerization yield, in both the optimization and anti-optimization experiments, were due to control of the intrinsic isomerization efficiency rather than to modulation of the excited-state population. Selective coupling of the applied electric field to vibrational modes appears to be involved in controlling the reaction.

From the time profiles of the shaped pulses, one can get an appreciation of the driving force provided by the applied electric field to gain insight into the mechanism. In order to better elucidate the details of the underlying shaped electric fields that drive the molecular coherences, we used a Wigner transform (*27*) to uncover the instantaneous frequency profile of the pulse shape

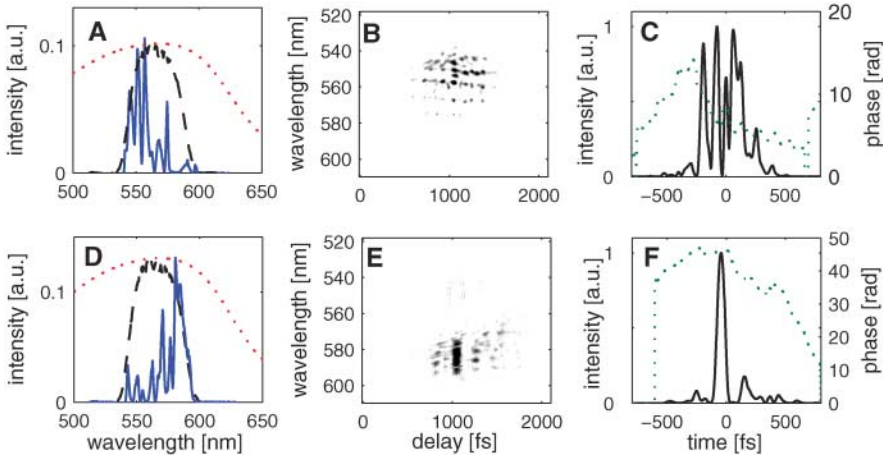

Fig. 3. (**A**) Spectral profile of the optimal excitation pulse (solid blue line), the transform-limited (19 fs FWHM) pulse (black dashed line), and bR transmittance spectrum (red dotted line). (**B**) Measured FROG trace for the optimal pulse. (**C**) Retrieved intensity (solid line) and phase profile (dashed line) from the FROG trace. (**D** to **F**) Corresponding data for the anti-optimal pulse. a.u., arbitrary units; rad, radians.

(fig. S3). According to these plots, the optimal pulse has a main temporal modulation with a period of 145 fs (230 ± 14 cm^{-1}), whereas the anti-optimal pulse is modulated by a period of approximately 215 fs (155 cm^{-1}). The optimal pulse has a modulation period that is resonant with the low-frequency torsional motions (and harmonics) in the excited state that are thought to be the key modes involved in the isomerization process, whereas the anti-optimal pulse is off resonance and thereby out of phase with this period. The exact modulation is more complex, involving different spectral components in the laser pulse that may be related to the non-Markovian dynamics of the involved vibrational modes. The most distinctive feature is the correspondence of the laser field modulation to one of the key modes involved in the reaction.

In the initial phase of the optimization experiments, we found that ΔA and thus the isomerization efficiency were slightly higher when the excitation pulse had randomly distributed phases and amplitudes than when it was transform-limited. This observation is very unusual and surprising (more than 20 optimization experiments were carried out in order to confirm this effect). No such effect has been observed in solvated organic molecules (*22*). In this regard, the photoisomerization process involves the displacement of more than one vibrational mode of retinal along the reaction coordinate (predominantly torsional and bond stretching character between C13 and C14), but not all vibrational modes uniformly; and this process is in strong competition with very fast nonradiative relaxation back to the ground state. We speculate that the protein structure may be biased to the displacement of the reactive modes preferentially along the reaction coordinate, in which case, sparse excitation to populate these modes may be favored over excitation of single vibrations or many unreactive modes that would steer the system away from the conical intersection or barrier crossing for reaction. In any case, this observation explains how the pulse optimization process avoided simple control of the excited-state population. There is a strong built-in bias for the photoreaction.

Transient kinetics. Transient kinetics (Figs. 4 and 5) were measured at the sample at variable delay times (within a 5- to 600-ps window) after excitation with the transform-limited, optimal, and anti-optimal pulses (all with equivalent actinic energies of 15.1 nJ ± 1%). The changes in isomerization efficiency had a stationary character (the absorption changes were constant within the 20- to 600-ps delay window), and the differences in the magnitudes of ΔA were ~20% (500-ps delay at 630 nm) relative to the difference spectrum observed upon excitation with the transform-limited pulse (Fig. 5). These magnitudes are smaller than those obtained during the optimization experiments (most likely because of differences in the samples used); however, they are still within the absolute accuracy of measurements. The distinction in pump-probe kinetics within the first ~5 ps after the excitation pulses is noteworthy, especially with excitation using the anti-optimal pulse. The difference in the population kinetics across the three pulses is present not only in the traces displayed in Fig. 5A, but in the whole investigated spectral range. In the delay window corresponding to the overlap of the probe pulse (~30 fs FWHM) with the excitation pulses, we clearly detected the presence of specific periodic modulations in pump-probe signals driven by the optimal and anti-optimal pulses (Fig. 4, B and C). Coupling of the optimal light pulse to specific vibrational modes resulted in the appearance of 195 ± 15 cm^{-1} oscillations with substantial amplitude (±30% of the maximal bleaching) in pump-probe kinetics (Fig. 4, B1 and B2). In contrast, in the pump-probe kinetics driven by the anti-optimal pulse, the observed oscillation had an aperiodic character (Fig. 4, C1 and C2) and strong positive chirp. The manifestation of strong oscillations in the pump-probe kinetics (quantum beats) clearly indicates a coherent excitation of the vibrational states (*28*) by the optimal pulse. Taking into account the results of previous studies of the retinal and bR vibrational structure (*29*, *30*), we posit that such an excitation pulse selectively and efficiently drives the ~200 cm^{-1} torsional mode in retinal by keeping the corresponding molecular vibrational mode in a coherent state during the excitation cycle (~300 fs) of the shaped pulse, and thus enhances the isomerization yield. We are effectively creating a specific superposition of vibrational modes (the so-called vibrational wave packet) on the excited-state surface that then propagates to the reactive crossing and is better tuned to the reaction. This enhancement of specific Raman-active modes has recently been experimentally demonstrated (*31*), using "open-loop" control to generate temporally periodic pulses that were resonant with the vibrational period of the desired mode (a train of several pulses spaced apart in time and frequency domains to be in resonance with this mode).

We emphasize the similarity between the temporal/spectral profile of the oscillations derived from the two-dimensional (2D) transient

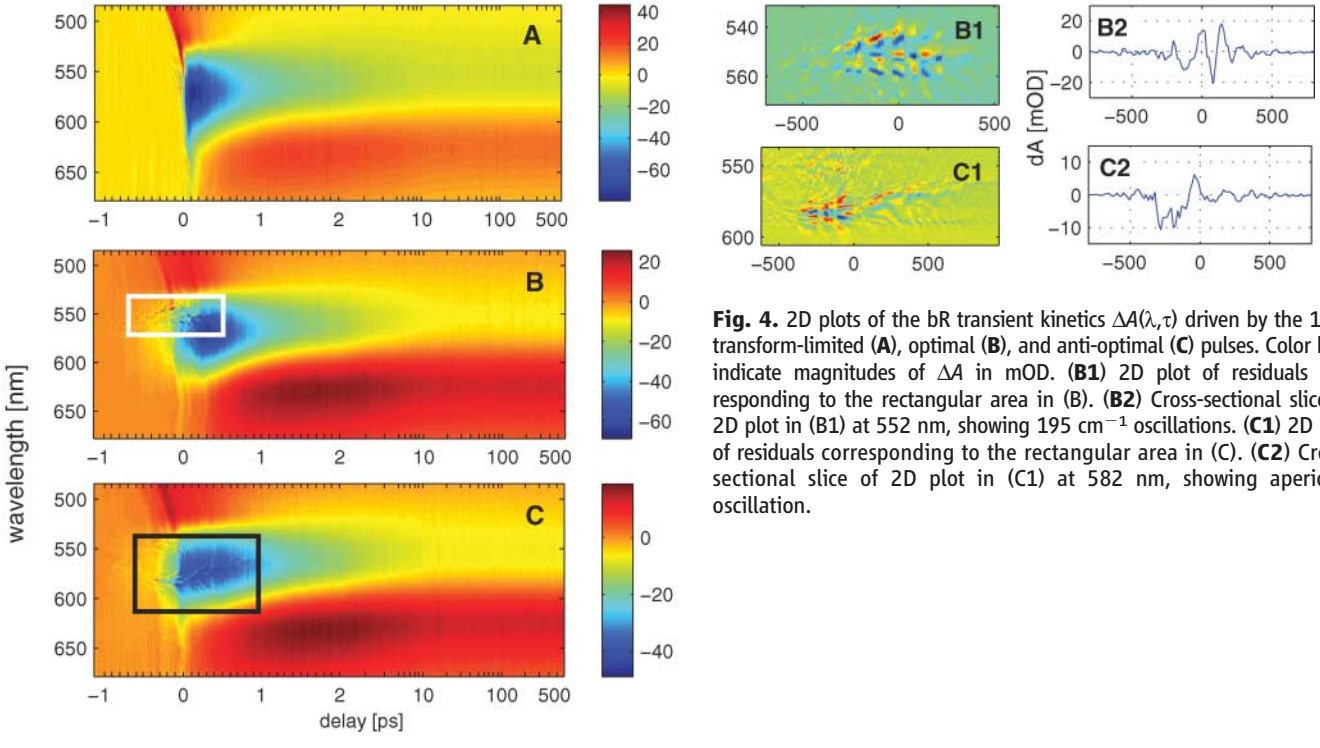

Fig. 4. 2D plots of the bR transient kinetics $\Delta A(\lambda,\tau)$ driven by the 19-fs transform-limited (**A**), optimal (**B**), and anti-optimal (**C**) pulses. Color bars indicate magnitudes of ΔA in mOD. (**B1**) 2D plot of residuals corresponding to the rectangular area in (B). (**B2**) Cross-sectional slice of 2D plot in (B1) at 552 nm, showing 195 cm^{-1} oscillations. (**C1**) 2D plot of residuals corresponding to the rectangular area in (C). (**C2**) Cross-sectional slice of 2D plot in (C1) at 582 nm, showing aperiodic oscillation.

kinetics (Fig. 4, B1 and C1) and the Wigner plots of the optimized pulses (*21*). The latter projections provide a visual portrayal of these key features of the shaped excitation fields.

Isomerization efficiency. At probe delays long enough to ensure completion of the K-intermediate buildup and full relaxation of unreacted all-trans retinal molecules to the ground state, the differential absorption spectrum was determined by absorption cross sections of the product isomer $\sigma_{cis}(\lambda)$ and the initial reactant $\sigma_{trans}(\lambda)$

$$\Delta A(\lambda) \propto \eta_{IY}[\sigma_{cis}(\lambda) - \sigma_{trans}(\lambda)]A_0 \quad (1)$$

where η_{IY} is the isomerization efficiency. A_0 is proportional to the number of initially excited all-trans retinal molecules and can be determined from the pump-probe kinetics driven by an impulsive excitation from the initial bleaching at zero delay [the absorption and excited-state emission spectra in bR are well separated (*10*), and thus the transient kinetics in the 540- to 600-nm window are not affected by stimulated emission]. Using the measured in situ absorption cross section $\sigma_{trans}(\lambda)$, the K-intermediate spectra can be straightforwardly derived from the ΔA spectra measured at a delay of 500 ps (Fig. 5B) by applying Eq. 1. Such decomposition (initial bleaching A_0 = –78 milli–optical density (mOD), using the19-fs pulse excitation) reproduces, within experimental accuracy, identical spectral shapes for the K intermediate and equal ratios [$\max(\sigma_{cis})/\max(\sigma_{trans})$ = 0.91 ± 0.01] if the isomerization yields η_{IY} are input as 78, 65, and 52% for the optimal, transform-limited, and anti-optimal pulses, respectively (fig. S4). Thus, the control of the absolute isomerization yield in bR using tailored excitation pulses is achieved over an absolute range of (78 – 52)/65 = 40%. The ratio between the maxima of the absorption cross sections for all-trans and 13-cis bR forms, as well as the position (585 nm) and shape of the band with $\max(\sigma_{cis})$, are in good agreement with the previously resolved transient spectra for these states (*19*).

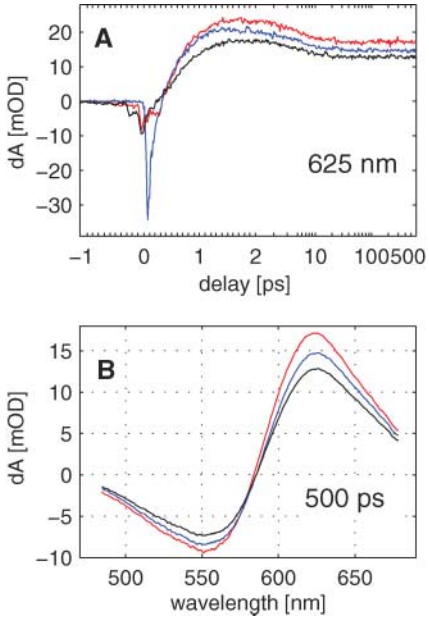

Fig. 5. (**A**) Decay traces at 625 nm measured in a 600-ps delay window after excitation with the optimal (red), transform-limited 19-fs FWHM (blue), and anti-optimal (black) pulses. (**B**) Differential absorption spectra $\Delta A(\lambda)$ acquired 500 ps after excitation [color scheme is as in (A)].

Energy dependence of isomerization and phase sensitivity. Our experiments were designed to test for quantum interference effects within biological systems. These studies must be conducted under weak field conditions in order to ensure that the same electronic levels are probed as in the actual biological processes. Ideally, these experiments should be conducted within the linear response with respect to the excitation energy to avoid any possible multiphoton processes. In the low–excitation energy limit, an isolated quantum system with a finite number of eigenstates, such as a small molecule in vacuum, should generally be insensitive to the phase information contained in the excitation light (*1*). Such a "closed" quantum system is always in a pure state (a coherent superposition of eigenstates) that can be described using the Schrödinger equation and wave function formalism (*32*). The retinal molecule in a protein environment belongs to the class of "open" systems, wherein the molecule/environment (system/bath) interaction leads to dephasing of the system states and energy redistribution among them, creating mixed states. Coherent control of such open systems is a difficult problem to treat theoretically because it requires specific information about the bath interactions that is generally not known. However, very recently the manipulation of the excited-state population in an open system (a molecule in a solvent) was experimentally demonstrated, and the phase sensitivity in the weak excitation limit (only 1 molecule in ~500 absorbing a photon during the excitation cycle) was revealed (*22*). The phase sensitivity of the excited-state population in dissipative systems was further modeled numerically (*33*), and the selective excitation of Raman active modes in the excited state in this regime has also been demonstrated (*34*). These recent developments are consistent with our interpretation of exciting specific vibrations in the excited state that interfere at the reaction crossing point. However, the energy dependence and coherent nature of the excited modes need to be determined to ensure that the experiments are in the weak field limit for coherent control.

The fluence in the optimization experiments E_{exc} = 2.7 × 10^{14} photons/cm^2 was approximately 20 times lower than the level necessary to saturate the retinal $S_0 \rightarrow S_1$ transition in the protein environment, which can be estimated, using the known extinction coefficient (*35*) ε(560 nm) = 54000 M^{-1} cm^{-1}, to be E_s = 4.8 × 10^{15} photons/cm^2 (*36*). At this relatively low fluence, the ratio between excited and nonexcited molecules (per laser shot) can be estimated, using the Poisson distribution, to be 1:40, and ~1% of the measured signal can arise from two-photon processes such as cascaded absorption $S_1 \rightarrow S_n$ (*37*). Therefore, the influence of actinic pulse energy on the isomerization control efficiency was checked independently by measuring ΔA (630 nm) at a delay of 20 ps for a wide range of pulse energies (Fig. 6A). Coherent control of the isomerization efficiency is clearly operative at the lower energies. Figure 6B shows the corresponding isomerization yield dependencies, defined as $IY(E_{exc}) \propto \Delta A/E_{exc}$. There is a slight nonlinearity to the dependence at a high actinic energy level. However, the isomerization efficiency depends strongly on the excitation pulse shape even for a pulse energy less than 1 nJ, which corresponds to the excitation of 1 bR out of ~300 per laser shot. Another order-of-magnitude reduction in actinic excitation energy with an improvement in signal-to-noise ratio (which is physically limited by

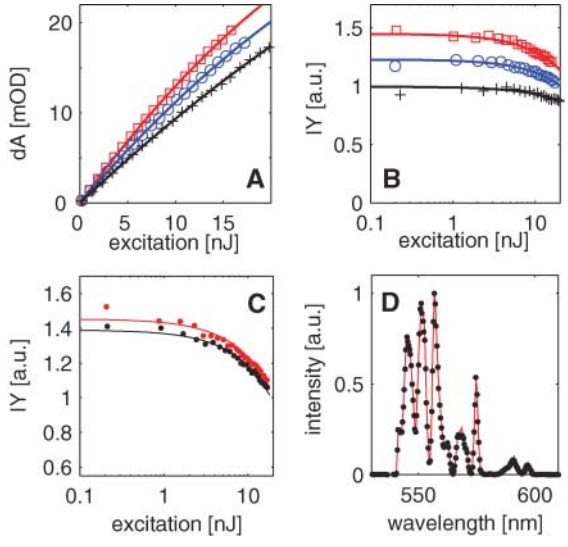

Fig. 6. Energy dependence of (**A**) the ΔA signal, measured at 630 nm 20 ps after excitation, and (**B**) the corresponding isomerization yields. Both plots show results for the optimal (red), anti-optimal (black), and transform-limited (blue) pulses. A quadratic fit (solid lines) shows the energy dependence to be essentially linear at low energies, with a small deviation (due to saturation of the absorbance) of less than 18% at the highest excitation energy. (**C**) Isomerization yields versus excitation energy for the optimal pulse with the phase modulation (red points) and without it (black points), showing a phase sensitivity of isomerization. Lines are quadratic fits. (**D**) Comparison of the spectral profiles of the optimal pulse with (red line) and without (black points) phase modulation. Spectral shapes are essentially identical, and thus the fluence dependencies $\Delta A(E_{exc})$ can be compared directly.

intrinsic light scattering in bR) will help establish the exact nature of the field interaction. The main conclusion is that the experiment is clearly in the weak field limit and the laser field is not strongly perturbing the underlying thermally populated modes, but rather inducing their interference in the excited-state surface. Isomerization yields were also compared with and without phase control (Fig. 6C), keeping spectral amplitudes constant (Fig. 6D; spectral profiles were confirmed using a tunable monochromator with 0.2-nm spectral resolution). The data show a clear phase dependence indicative of coherent control.

Pure amplitude modulation alters the temporal profile of the pulse (fig. S5); therefore, removing the phase modulation affects the isomerization yield by only 5 to 7%. The phase sensitivity of the control efficiency further illustrates the coherent nature of the state preparation.

The temporal profiles of the shaped optimal and anti-optimal pulses and the observed degree of the isomerization yield control are consistent with the known fast electronic dephasing of bR (*10*, *38*). The largest field amplitudes are confined to approximately 300-fs widths to yield 20% control. In the case of transform-limited pulses, all the vibrational levels within the excitation bandwidth are excited in phase and there is a fast decoherence in the initial electronic polarization (*38*). However, with the phase-selective restricted bandwidths in the shaped pulses, there is an opportunity to manipulate different vibrational states with much longer coherence times than the electronic polarization. The resultant constructive and destructive interference effects involving vibrational modes displaced along the reaction coordinate offer the possibility of controlling isomerization. Experimental observations presented here show that the wave properties of matter can play a role in biological processes, to the point that they can even be manipulated.

References and Notes

1. M. Shapiro, P. Brumer, *Rep. Prog. Phys.* **66**, 859 (2003).
2. S. H. Shi, H. Rabitz, *J. Chem. Phys.* **92**, 364 (1990).
3. W. T. Pollard, S. Y. Lee, R. A. Mathies, *J. Chem. Phys.* **92**, 4012 (1990).
4. Q. Wang, R. W. Schoenlein, L. A. Peteanu, R. A. Mathies, C. V. Shank, *Science* **266**, 422 (1994).
5. K. C. Hasson, F. Gai, P. A. Anfinrud, *Proc. Natl. Acad. Sci. U.S.A.* **93**, 15124 (1996).
6. T. Ye *et al.*, *J. Phys. Chem. B* **103**, 5122 (1999).
7. R. Gonzalez-Luque *et al.*, *Proc. Natl. Acad. Sci. U.S.A.* **97**, 9379 (2000).
8. T. Kobayashi, T. Saito, H. Ohtani, *Nature* **414**, 531 (2001).
9. J. Herbst, K. Heyne, R. Diller, *Science* **297**, 822 (2002).
10. J. T. M. Kennis *et al.*, *J. Phys. Chem. B* **106**, 6067 (2002).
11. S. Hayashi, E. Tajkhorshid, K. Schulten, *Biophys. J.* **85**, 1440 (2003).
12. S. C. Flores, V. S. Batista, *J. Phys. Chem. B* **108**, 6745 (2004).
13. Y. Ohtsuki, K. Ohara, M. Abe, K. Nakagami, Y. Fujimura, *Chem. Phys. Lett.* **369**, 525 (2003).
14. G. Vogt, G. Krampert, P. Niklaus, P. Nuernberger, G. Gerber, *Phys. Rev. Lett.* **94**, 068305 (2005).
15. K. Hoki, P. Brumer, *Phys. Rev. Lett.* **95**, 168305 (2005).
16. J. L. Herek, W. Wohlleben, R. J. Cogdell, D. Zeidler, M. Motzkus, *Nature* **417**, 533 (2002).
17. J. Tittor, D. Oesterhelt, *FEBS Lett.* **263**, 269 (1990).
18. S. L. Logunov, M. A. El-Sayed, *J. Phys. Chem. B* **101**, 6629 (1997).
19. H. J. Polland *et al.*, *Biophys. J.* **49**, 651 (1986).
20. F. Gai, K. C. Hasson, J. C. McDonald, P. A. Anfinrud, *Science* **279**, 1886 (1998).
21. See supporting data on *Science* Online.
22. V. I. Prokhorenko, A. M. Nagy, R. J. D. Miller, *J. Chem. Phys.* **122**, 184502 (2005).
23. A. K. Dioumaev, V. V. Savransky, N. V. Tkachenko, V. I. Chukharev, *J. Photochem. Photobiol. B Biol.* **3**, 397 (1989).
24. G. Schneider, R. Diller, M. Stockburger, *Chem. Phys.* **131**, 17 (1989).
25. A. Xie, *Biophys. J.* **58**, 1127 (1990).
26. S. P. Balashov, E. S. Imasheva, R. Govindjee, T. G. Ebrey, *Photochem. Photobiol.* **54**, 955 (1991).
27. J. Paye, *IEEE J. Quant. Electron.* **28**, 2262 (1992).
28. H. L. Fragnito, J.-Y. Bigot, P. C. Becker, C. V. Shank, *Chem. Phys. Lett.* **160**, 101 (1989).
29. A. B. Myers, R. A. Harris, R. A. Mathies, *J. Chem. Phys.* **79**, 603 (1983).
30. B. X. Hou, N. Friedman, M. Ottolenghi, M. Sheves, S. Ruhman, *Chem. Phys. Lett.* **381**, 549 (2003).
31. R. Morita, M. Yamashita, A. Suguro, H. Shigekawa, *Opt. Commun.* **197**, 73 (2001).
32. K. Blum, *Density Matrix Theory and Applications* (Plenum, New York, 1981).
33. D. Gelman, R. Kosloff, *J. Chem. Phys.* **123**, 234506 (2005).
34. J. Hauer, H. Skenderovic, K.-L. Kompa, M. Motzkus, *Chem. Phys. Lett.* **421**, 523 (2006).
35. D. Oesterhelt, W. Stoeckenius, in *Methods in Enzymology*, vol. 31 of *Biomembranes* (Academic Press, New York, 1974), pp. 667–678.
36. The saturation energy is related to the absorption cross section σ as $E_s = 1/\sigma_{trans}$ (for a negligibly small contribution of the excited-state emission), and σ is related to the extinction coefficient ε as $\sigma = [\log(10)/N_A]\varepsilon = 3.86 \times 10^{-21}\varepsilon$, where N_A is Avogadro's number.
37. The fraction of excited molecules can be estimated as a ratio between the number of absorbed photons $n_p = E_{exc} \times \pi d_0^2/4$ and the number of retinal molecules $N_m = C \times V$ in an excited volume $V_0 \cong l_0 \times \pi d_0^2/4$, where the concentration is $C = 2.303A_0/\sigma_{trans}$, A_0 is OD at 565 nm (0.9), $l_0 = 0.04$ cm is the path length in the cell used, and $d_0 = 0.015$ cm is the beam diameter in the sample. This gives a fraction of excited molecules of 0.0236 (that is, 1 out of 42.3 molecules will be excited during the excitation pulse at a given fluence). The fraction of double-excited molecules can be estimated from the Poisson distribution $f(k) = e^{-\lambda}(\lambda)^k/k!$, where $\lambda = 0.0236$, and k is the number of occurrences ($k = 1$ for the single excitation, $k = 2$ for the double excitation, etc.). Thus, the fraction of double-excited molecules $f(2)/f(1) = \lambda/2$; that is, 1.18%.
38. V. F. Kamalov, T. M. Masciangioli, M. A. El-Sayed, *J. Phys. Chem.* **100**, 2762 (1996).
39. K. Edman *et al.*, *Nature* **401**, 822 (1999).

40. This work was supported by the National Sciences and Engineering Research Council of Canada. The authors thank J.T.M. Kennis, Vrije Universiteit Amsterdam, for helpful discussions of preliminary results.

Supporting Online Material

www.sciencemag.org/cgi/content/full/313/5791/1257/DC1
Materials and Methods
Figs. S1 to S5
References

1 June 2006; accepted 10 August 2006
10.1126/science.1130747

Phytophthora Genome Sequences Uncover Evolutionary Origins and Mechanisms of Pathogenesis

Brett M. Tyler,[1*] Sucheta Tripathy,[1] Xuemin Zhang,[1] Paramvir Dehal,[2,3] Rays H. Y. Jiang,[1,4] Andrea Aerts,[2,3] Felipe D. Arredondo,[1] Laura Baxter,[5] Douda Bensasson,[2,3,6] Jim L. Beynon,[5] Jarrod Chapman,[2,3,7] Cynthia M. B. Damasceno,[8] Anne E. Dorrance,[9] Daolong Dou,[1] Allan W. Dickerman,[1] Inna L. Dubchak,[2,3] Matteo Garbelotto,[10] Mark Gijzen,[11] Stuart G. Gordon,[9] Francine Govers,[4] Niklaus J. Grunwald,[12] Wayne Huang,[2,14] Kelly L. Ivors,[10,15] Richard W. Jones,[16] Sophien Kamoun,[9] Konstantinos Krampis,[1] Kurt H. Lamour,[17] Mi-Kyung Lee,[18] W. Hayes McDonald,[19] Mónica Medina,[20] Harold J. G. Meijer,[4] Eric K. Nordberg,[1] Donald J. Maclean,[21] Manuel D. Ospina-Giraldo,[22] Paul F. Morris,[23] Vipaporn Phuntumart,[23] Nicholas H. Putnam,[2,3] Sam Rash,[2,13] Jocelyn K. C. Rose,[24] Yasuko Sakihama,[25] Asaf A. Salamov,[2,3] Alon Savidor,[17] Chantel F. Scheuring,[18] Brian M. Smith,[1] Bruno W. S. Sobral,[1] Astrid Terry,[2,13] Trudy A. Torto-Alalibo,[1] Joe Win,[9] Zhanyou Xu,[18] Hongbin Zhang,[18] Igor V. Grigoriev,[2,3] Daniel S. Rokhsar,[2,7] Jeffrey L. Boore[2,3,26,27]

Draft genome sequences have been determined for the soybean pathogen *Phytophthora sojae* and the sudden oak death pathogen *Phytophthora ramorum*. Oömycetes such as these *Phytophthora* species share the kingdom Stramenopila with photosynthetic algae such as diatoms, and the presence of many *Phytophthora* genes of probable phototroph origin supports a photosynthetic ancestry for the stramenopiles. Comparison of the two species' genomes reveals a rapid expansion and diversification of many protein families associated with plant infection such as hydrolases, ABC transporters, protein toxins, proteinase inhibitors, and, in particular, a superfamily of 700 proteins with similarity to known oömycete avirulence genes.

Phytophthora plant pathogens attack a wide range of agriculturally and ornamentally important plants (*1*). Late blight of potato caused by *Phytophthora infestans* resulted in the Irish potato famine in the 19th century, and *P. sojae* costs the soybean industry millions of dollars each year. In California and Oregon, a newly emerged *Phytophthora* species, *P. ramorum*, is responsible for a disease called sudden oak death (*2*) that affects not only the live